RAPID COMMUNICATIONS

PHYSICAL REVIEW E **90**, 030402(R) (2014)

Directed self-organization of quantum dots

Jean-Noël Aqua[*] and Xianbin Xu

UPMC Univ Paris 06, UMR 7588, Institut des Nano-Sciences de Paris (INSP) 4 place Jussieu, Paris, France
and CNRS, INSP, UMR 7588, 4 place Jussieu, Paris, France

(Received 7 June 2013; revised manuscript received 24 July 2014; published 25 September 2014)

We devise a nonlinear dynamical model of the growth of strained islands on a pattern. We study the morphological instability of a thin film that develops with a characteristic wavelength in the presence of an external forcing due to an underlying patterned substrate with another wavelength. We find in some conditions that the islands can form in well-organized arrays located on either the peaks or valleys of the pattern depending on the film thickness and ratio of the two characteristic wavelengths. These results are rationalized by a kinetic phase diagram and correlated with the morphology when the islands and the wetting layer grow. We find that the islands may be ordered and homogeneous when their coarsening is significantly slowed down, in agreement with experimental observations reported in the literature.

DOI: 10.1103/PhysRevE.90.030402 PACS number(s): 81.15.Hi, 46.70.Lk, 68.35.Ct, 81.10.Aj

The homogeneity and order of an assembly of nanostructures are crucial for their use in large-scale electronic or optical systems. They challenge our understanding and control of growth at small scales. Quantum dots grown on strained crystalline films in coherent epitaxy after a two-dimensional to three-dimensional strain-relieving transition usually exhibit strong size fluctuations (see, e.g., [1]) related to their intrinsically stochastic nucleation origin. By avoiding this stochastic stage, islands resulting from an instability with long-range order are *a priori* good candidates for achieving uniform properties. This is especially the case for the nucleationless Asaro-Tiller-Grinfel'd instability of strained films, which develops, e.g., in the paradigmatic SiGe systems [2,3]. Unfortunately, the resulting islands also exhibited a poor homogeneity due to fluctuations and coarsening [4].

To reduce inhomogeneities, the growth of islands on morphologically patterned substrates was extensively studied [5]. It leads to uniform assemblies of well-ordered islands [6], but contradictory results are found under comparable conditions: Ge islands on Si(001) grow either on top or at the edge of the pattern [7–10], on sidewalls [11], inside pits [12], or both inside pits and on terraces [13]. Theoretical analyses focused mainly on equilibrium [12,14–17]: Finite-element strain calculations showed that islands minimize their energy inside pits with shallow enough sidewall angles [18], while Monte Carlo simulations indicated that islands minimize their energy on terraces rather than on pit walls [19]. However, so far, no dynamical analysis rationalizes the possibility of islands sitting on either the crests or troughs of the pattern, revealing the incomplete understanding of the growth mechanisms and the difficult comparison between theory and experiments even in such paradigmatic systems [17,20,21].

We investigate in this Rapid Communication the long-time nonlinear evolution of the morphological Asaro-Tiller-Grinfel'd instability [2] on a pattern. On a flat pattern, the instability leads to the self-organization of islands with a characteristic wavelength that is in competition here with the order enforced by the pattern with a tunable wavelength. Due to the analytical solution for the elastic field of the buried and patterned film-substrate interface, we numerically solve the surface diffusion equation on large systems and systematically analyze the resulting morphologies. We characterize the relevant parameters dictating the islands' positions and characteristics. They result from the kinetic competition between elastic and wetting interactions and are related to the slowdown of ripening, due to crystalline anisotropy and reinforced here by patterning.

Dynamical model. We study a crystalline film bounded by the free surface at $z = h(\boldsymbol{r},t)$ and the film-substrate interface at $z = \eta(\boldsymbol{r})$ where $\boldsymbol{r} = (x,y)$ (Fig. 1). The morphological evolution results from the surface diffusion ruled by

$$\frac{\partial h}{\partial t} = D\boldsymbol{\Delta}[\mu^{\rm el} - \gamma\,\boldsymbol{\Delta} h + \mu_w + \mu_{\rm anis}] + F, \qquad (1)$$

with the diffusion coefficient D, the deposition flux F, and the elastic energy density μ^{el}. The surface energy $\gamma = \gamma_w(h) + \gamma_{\rm anis}(\boldsymbol{n})$ depends here on the film height h and surface local orientation $\boldsymbol{n}$ [22,23] in order to describe the wetting and anisotropic effects $\mu_{w({\rm anis})} = \frac{\delta}{\delta h}\int d^2S\,\gamma_{w({\rm anis})}$. Wetting describes the influence of the film-substrate interface on the free surface energetics and is crucial to describe the growth of strained films [24]. It occurs for thicknesses of the order of a few atomic lengths. It is described here by

$$\gamma_w = \gamma_f[1 + c_w \exp(-H/\delta_w)] \qquad (2)$$

and depends on the local thickness $H(\boldsymbol{r}) = h(\boldsymbol{r}) - \eta(\boldsymbol{r})$, with the film surface energy γ_f and the parameters c_w,δ_w, which can be derived from *ab initio* calculations [25] or comparison with experimental results [26]. Such a wetting effect inhibits the surface morphological instability below a critical thickness H_c (typically a few nanometers) and leads to the formation of a wetting layer in agreement with experiments. In addition to wetting, anisotropy is also crucial in such crystalline films and is mainly at work in the surface energy dependence on the local orientation $\boldsymbol{n}$. In order to depict experimental findings on SiGe [26,27], we use an anisotropic function $\gamma_{\rm anis}(\boldsymbol{n})$ describing a shallow (001) minimum and stiff (105) orientations, but the following results are mostly due to the existence of the preferential stiff orientations. Finally, the pattern crucially affects elasticity and we generalize the computation of [26]

---

[*] aqua@insp.jussieu.fr

1539-3755/2014/90(3)/030402(5)

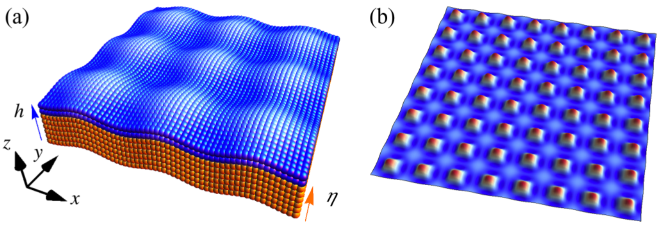

FIG. 1. (Color online) (a) Film with a free surface at $z = h(x,y,t)$ deposited on a pattern at $z = \eta(x,y)$. (b) Best-ordered stationary islands sitting in the pattern valleys, resulting from the numerical integration of Eq. (1) for $\lambda_\eta/\lambda_{\rm ATG} = 1$ and $\bar{H}/H_c = 1.8$.

to a patterned geometry by solving analytically mechanical equilibrium in the small-slope approximation. The film-substrate interface is coherent, so displacements propagate throughout the system due to the misfit m between the film and substrate. A flat film is characterized by the elastic energy density $\mathcal{E}_0 = 2Ym^2(1+\nu)/(1-\nu)$, with the Young modulus Y, Poisson ratio ν, and characteristic length $l_0 = \gamma_f/\mathcal{E}_0$. Up to second order in the slope, $\mu^{\rm el} = \mu_0 + \mu_1 + \mu_2 + \cdots$, where

$$\mu_1/\mathcal{E}_0 = -\mathcal{H}_{ii}[h] + \mathcal{B}[\mathcal{H}_{ii}[\eta]], \qquad (3)$$

with summation over $i = x,y$. Surface relaxation is associated with the operator $\mathcal{H}$ defined in Fourier space along $\boldsymbol{r}$ by $\mathcal{H}_{ij}[h] = (k_i k_j/|\boldsymbol{k}|)\tilde{h}(\boldsymbol{k})$ while the damping of the buried film-substrate dipoles is associated with $\mathcal{B}[h] = \exp(-|\boldsymbol{k}|\bar{H})\tilde{h}(\boldsymbol{k})$ with $\bar{H} = \langle H(\boldsymbol{r})\rangle$. The linear instability analysis of (1) shows that above some critical thickness H_c, a harmonic modulation $H(\boldsymbol{r},t) = \bar{H} + \epsilon\exp(\mathrm{i}\boldsymbol{k}\cdot\boldsymbol{r} + \sigma t)$ has a positive growth rate σ for an interval of wave vectors and is maximum for a given $k_{\rm ATG}$, which defines the instability wavelength $\lambda_{\rm ATG} = 2\pi/k_{\rm ATG}$ [26]. At second order we find $\mu_2/\mathcal{E}_0 = \mu_2^{hh} + \mu_2^{h\eta} + \mu_2^{\eta\eta}$ with

$$\begin{aligned}
\mu_2^{\eta\eta} &= -\mathcal{B}[\eta\boldsymbol{\Delta}\eta + |\boldsymbol{\nabla}\eta|^2] + \mathcal{B}[\mathcal{H}_{ij}[\eta]]\theta_{ij}^{kl}\mathcal{B}[\mathcal{H}_{kl}[\eta]],\\
\mu_2^{h\eta} &= -h\mathcal{B}[\boldsymbol{\Delta}\eta] - 2\mathcal{H}_{ij}[h]\theta_{ij}^{kl}\mathcal{B}[\mathcal{H}_{kl}[\eta]]\\
&\quad -2\mathcal{H}_{ij}\big[h\theta_{ij}^{kl}\mathcal{B}[\mathcal{H}_{kl}[\eta]]\big], \qquad (4)
\end{aligned}$$

while μ_2^{hh} and the geometrical tensor θ_{ij}^{kl} are given in [22]. Given the solution of the elastic problem (3) and (4), the evolution may be efficiently computed on large scales due to the numerical resolution of (1). Initially, $h(\boldsymbol{r},t=0) = \eta(\boldsymbol{r})$ and we consider deposition[1] up to $\bar{H}$ for a given $\bar{t}$ (we only consider thin films in the following); after deposition, annealing ($F = 0$) is considered. A long enough annealing allows the system to enter its nonlinear regime where quantum dots eventually self-organize [28]. However, as observed on as-grown films [23], the morphological instability does not significantly grow during deposition and is well described by the linearization of (1). Hence, in the instability nucleationless framework, the deposition flux F and temperature T are irrelevant parameters [linearly, (1) is trivially invariant under the change $z \to z - Ft$ [29]].[2]

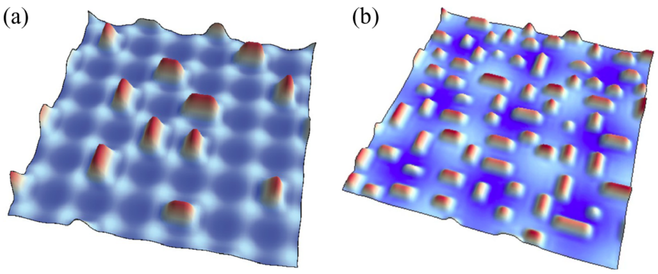

FIG. 2. (Color online) Stationary morphologies with low spatial order for (a) islands in the valleys having undergone coarsening for $\lambda_\eta/\lambda_{\rm ATG} = 1$ and $\bar{H}/H_c = 1.3$ and (b) disordered islands similar to the self-organized islands on a flat substrate for $\lambda_\eta/\lambda_{\rm ATG} = 6$ and $\bar{H}/H_c = 1.8$.

Results. The surface evolution results from the balance between (i) the surface energy $-\gamma\boldsymbol{\Delta}h$ minimum in the film valleys (where atoms are more coordinated), (ii) the elastic relaxation of the free surface $-\mathcal{H}_{ii}[h] + \mu_2^{hh}$ minimum on the surface peaks [both (i) and (ii) are independent of the pattern], (iii) the relaxation of the buried dipole $\mathcal{B}[\mathcal{H}_{ii}[\eta]] + \mu_2^{\eta\eta}$ minimum over the vertical projection of the pattern valleys, (iv) the interference term $\mu_2^{h\eta}$, and (v) the wetting potential, which favors growth over the vertical projection of the pattern peaks. The variety of island locations found below proves that the system is not trivially driven by the pattern forcing or by a single effect.

We first study generically an egg-carton pattern $\eta(\boldsymbol{r}) = A[\cos(2\pi x/\lambda_\eta) + \cos(2\pi y/\lambda_\eta)]$ (Fig. 1). The instability with the characteristic length $\lambda_{\rm ATG}$ grows on top of the pattern with λ_η. Of special interest is the ratio $\lambda_\eta/\lambda_{\rm ATG}$, which rules the growth rate σ_η of the initial profile, while the thickness $\bar{H}$ rules both the wetting and the buried dipoles interactions. As found on unpatterned substrates, the combination of anisotropy, elasticity, and wetting leads to a significant slowdown in Ostwald coarsening [26] sometimes after some partial ripening. It is so efficient that nearly stationary morphologies, i.e., pyramids with (105) facets, result after some time, as found in experiments [26]. The following results correspond to $c_w = 0.1$, $\delta_w = 0.01$, and $A/l_0 = 0.1$ but are generic.[3] We first depict our findings before rationalizing them.

We consider the wavelength coincidence $\lambda_\eta = \lambda_{\rm ATG}$ (see Figs. 1 and 2). For large enough $\bar{H}/H_c$, pyramidal islands quickly arise after the initial instability, grow, and remain in the valleys of the pattern, forming the best organized arrays [Fig. 1(b)]. Each island grows in one valley and gathers a rather uniform volume, reducing the chemical potential differences between islands and thence coarsening, thus consolidating their uniformity. The island size distribution (ISD) in the stationary state is narrow and significantly improved compared to the flat substrate case (Fig. 3). However, for $\bar{H}/H_c \gtrsim 1$, the first islands after the instability are still located in the valleys but are too small to have well-developed facets. They undergo coarsening, where the smallest islands disappear while the largest grow. Eventually, a stationary state occurs when the

---

[1] This is done by adding a white deposition noise on the right-hand side of (1).

[2] A dependence on F of the nonlinear quantum dots arises under constant deposition, but for thick films not studied here [29].

[3] They are relevant for $0.01 < A/l_0 < 0.4$, a pattern slope lower than (105), and $c_w = 0.05$, 0.1 and 0.2.

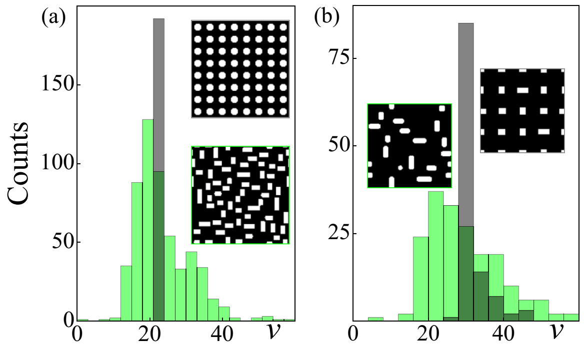

FIG. 3. (Color online) Island size distribution of stationary islands on a pattern (dark gray) and on a flat substrate (light green) for (a) $\lambda_\eta/\lambda_{\mathrm{ATG}} = 1$ and $\bar{H}/H_c = 1.8$ and (b) $\lambda_\eta/\lambda_{\mathrm{ATG}} = 2.7$ and $\bar{H}/H_c = 1.1$.

islands are large enough to have facets [see Fig. 2(a)] and thence small chemical potential differences [22].

For larger $\lambda_\eta/\lambda_{\mathrm{ATG}}$, similar results are found except when $\bar{H}/H_c \gtrsim 1$ (Fig. 4). There, islands grow and remain on the pattern peaks. Each peak is decorated by a single island when $\lambda_\eta/\lambda_{\mathrm{ATG}}$ is not too large and the ISD is narrow (Fig. 3). For larger $\lambda_\eta/\lambda_{\mathrm{ATG}}$, island clusters arise on the peaks as the matter available at each top becomes large compared to the typical volume of isolated islands. Finally, for large $\bar{H}/H_c$ and $\lambda_\eta/\lambda_{\mathrm{ATG}}$, mainly disordered morphologies fully similar to the self-organized islands observed on a flat substrate occur, as the influence of the pattern is small [Fig. 2(b)].

The stationary morphologies are summarized in the kinetic phase diagram Fig. 5 as a function of $\lambda_\eta/\lambda_{\mathrm{ATG}}$ and $\bar{H}/H_c$. For small $\lambda_\eta/\lambda_{\mathrm{ATG}}$, the initial corrugation with λ_η has a negative σ_η (capillarity overcomes relaxation) and shrinks after skipping to out of phase [labeled "bottom (stable)"]. For $\lambda_\eta/\lambda_{\mathrm{ATG}} > 1$, islands grow in the valleys for large $\bar{H}$ (bottom), but possibly on the peaks when $\bar{H}/H_c \gtrsim 1$ (top). Finally, for larger $\lambda_\eta/\lambda_{\mathrm{ATG}}$, clusters of islands arise on the peaks for thin films (clusters on top), while a disordered morphology occurs otherwise (disorder).

Initial evolution. To rationalize these findings, we investigate the initial instability through the linear solution of Eq. (1). Initially, the film follows the pattern in phase. When $\lambda_\eta/\lambda_{\mathrm{ATG}}$ is not too large and $\bar{H}/H_c$ not too small, the film skips in the linear regime from in to out of phase after some time t^{ex}. This phase exchange allows minimization of the elastic energy of the buried dipoles [20,30]. For larger $\lambda_\eta/\lambda_{\mathrm{ATG}}$, the k_{ATG} mode may become larger than the k_η mode at some time $t^{\max}$ before this phase shift (Fig. 6) and leads to a disorderedlike self-organized morphology. However, the linear solution describes only the initial evolution and we indicate in Fig. 6 the typical time when the islands emerge in the nonlinear regime, which also corresponds to the saturation of the surface roughness (Fig. 7).[4] (We find in our systematic analysis that the island localization in the stationary state (top, peak or disorder) corresponds to the morphology of the instability when the islands and the wetting layer form at the beginning of the nonlinear regime. It may be dictated either by the kinetics of the linear instability (with either the valley or peak of disordered positions) or mainly by wetting (with the peak position). When $\bar{H}/H_c \gtrsim 1$, the phase shift does not occur before the nonlinear wetting interactions come into play and enforce a peak position. Note that in some cases (especially for small $\bar{H}/H_c$), coarsening may cause the disappearance of some islands, either to the benefit of islands on similar positions or, when they coexist, from peaks to valleys where strain is more relaxed. For example, when

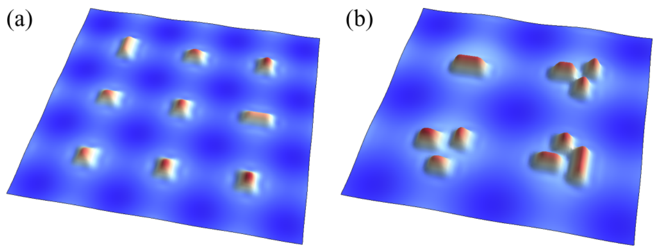

FIG. 4. (Color online) Stationary islands on top of the pattern peaks for (a) $\lambda_\eta/\lambda_{\mathrm{ATG}} = 2.7$ and $\bar{H}/H_c = 1.1$ and (b) $\lambda_\eta/\lambda_{\mathrm{ATG}} = 6$ and $\bar{H}/H_c = 1.1$.

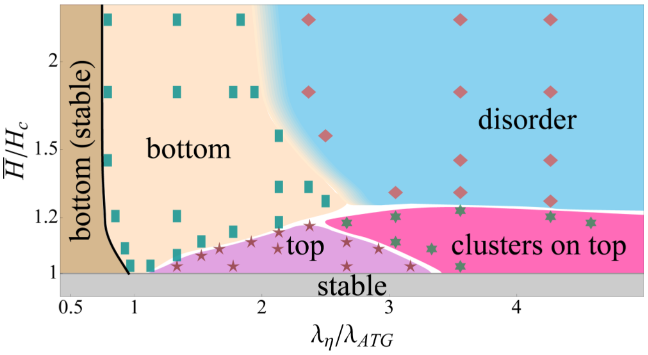

FIG. 5. (Color online) Kinetic phase diagram displaying the localization of islands grown on an egg-carton substrate as a function of the ratios of the film thickness to critical height $\bar{H}/H_c$ and the pattern to instability wavelengths $\lambda_\eta/\lambda_{\mathrm{ATG}}$. Symbols show the simulations that set the boundaries. The instability does not develop on the left side of the solid line and when $\bar{H} < H_c$.

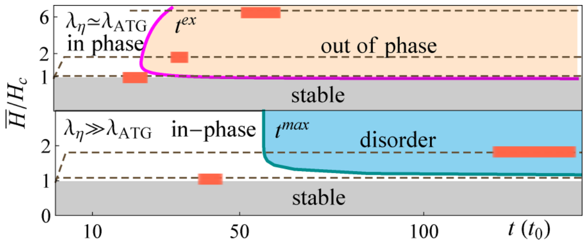

FIG. 6. (Color online) Typical evolution for $\lambda_\eta/\lambda_{\mathrm{ATG}} = 1.4$ (top) and $\lambda_\eta/\lambda_{\mathrm{ATG}} = 6$ (bottom), displaying the morphology as a function of time t and thickness $\bar{H}$. The dotted line represents the thickness evolution during deposition and annealing. Orange rectangles show the time when islands form. The t^{ex} line characterizes the shift from in to out of phase of the linear solution of (1) [30], while $t^{\max}$ characterizes the time when $h(k_{\mathrm{ATG}}) = h(k_\eta)$ for this solution [30].

---

[4] The linear evolution is made of exponentials and its initial decrease corresponds to the shift from in to out of phase [30].

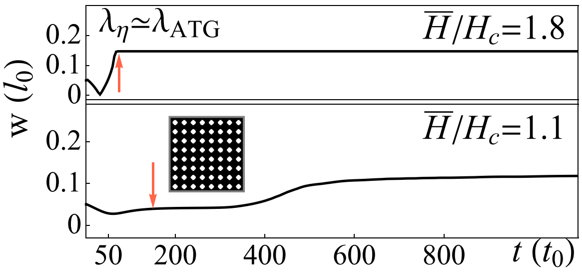

FIG. 7. (Color online) Evolution of the surface roughness w for $\lambda_\eta/\lambda_{ATG} = 1.4$ and $\bar{H}/H_c = 1.1$ and 1.8 (solid line). The islands' snapshot for $t = 200$ is displayed in the inset. Orange arrows indicate the time when well-defined islands appear.

$\lambda_\eta/\lambda_{ATG} = 1.4$ and $\bar{H}/H_c = 1.1$ (Fig. 7) the first islands to grow are isotropic and display a narrow ISD that lowers the coarsening driving force. The system evolves slowly before small fluctuations eventually lead to ripening and the formation of larger pyramids and coarsening is then again interrupted. Therefore, both anisotropy and the narrow ISD enforced by patterning cause the slowdown in coarsening.

Relation with experiments. A systematic experimental investigation of the island positioning as a function of λ_η and $\bar{H}$ in $Si_{1-x}Ge_x$ films ($x < 0.5$) on Si would be valuable to check the rationalization described in our model. Similarly to experiments [5,6], we find in some conditions uniform and ordered islands that do not coarsen and are located on either peaks or valleys of the pattern. Even if our model describes the nucleationless evolution observed in low-x films [3,26] and *a priori* not highly strained Ge films where nucleation is crucial [1,31,32], some mechanisms exhibited here could also be important in the nucleation case. Other parameters may also be important: (i) the pattern geometry that defines the surface initial condition; (ii) alloying, especially at high temperature [17,21]; and (iii) evaporation and condensation when epitaxy is not performed in high vacuum [33]. By considering a minimal model, our results are aimed at identifying the basic mechanisms at work.

In summary, we devised a dynamical model describing the morphological instability and subsequent quantum dot growth on a strained film on a pattern. We solve elasticity at nonlinear order to investigate the long-time dynamics. We found different regimes where islands form either ordered and uniform arrays on the pattern peaks or valleys or follow disordered morphologies, depending on the film thickness and ratio of the instability to the pattern length scales. The results were rationalized by the competition between the self-organization already at work on a flat substrate and the order enforced by the pattern. We showed that the buried dipoles and wetting interactions with opposite effects are the driving forces that control this directed self-organization. Extension of this work to other geometries and to the nucleation case using kinetic Monte Carlo simulations [34,35] could be interesting, especially in comparison with the present results.

Acknowledgments. The authors thank Thomas Frisch, Isabelle Berbezier, Jerry Floro, Paola Atkinson, and Christiane Caroli for fruitful discussions and insightful comments.

[1] D. J. Eaglesham and M. Cerullo, Phys. Rev. Lett. **64**, 1943 (1990); Y. W. Mo, D. E. Savage, B. S. Swartzentruber, and M. G. Lagally, *ibid.* **65**, 1020 (1990).

[2] R. J. Asaro and W. A. Tiller, Metall. Trans. **3**, 1789 (1972); M. A. Grinfeld, Sov. Phys. Dokl. **31**, 831 (1986).

[3] P. Sutter and M. G. Lagally, Phys. Rev. Lett. **84**, 4637 (2000); R. M. Tromp, F. M. Ross, and M. C. Reuter, *ibid.* **84**, 4641 (2000).

[4] See, e.g., J. A. Floro, M. B. Sinclair, E. Chason, L. B. Freund, R. D. Twesten, R. Q. Hwang, and G. A. Lucadamo, Phys. Rev. Lett. **84**, 701 (2000); S. Miyamoto, O. Moutanabbir, E. E. Haller, and K. M. Itoh, Phys. Rev. B **79**, 165415 (2009).

[5] J.-N. Aqua, I. Berbezier, L. Favre, T. Frisch, and A. Ronda, Phys. Rep. **522**, 59 (2013).

[6] M. Grydlik, G. Langer, T. Fromherz, F. Schäffler, and M. Brehm, Nanotechnology **24**, 105601 (2013).

[7] G. Jin, J. L. Liu, S. G. Thomas, Y. H. Luo, K. L. Wang, and B.-Y. Nguyen, Appl. Phys. Lett. **75**, 2752 (1999).

[8] T. Kitajima, B. Liu, and S. R. Leone, Appl. Phys. Lett. **80**, 497 (2002).

[9] B. Yang, F. Liu, and M. G. Lagally, Phys. Rev. Lett. **92**, 025502 (2004).

[10] P. D. Szkutnik, A. Sgarlata, S. Nufris, N. Motta, and A. Balzarotti, Phys. Rev. B **69**, 201309 (2004).

[11] Z. Zhong, A. Halilovic, M. Muhlberger, F. Schaffler, and G. Bauer, Appl. Phys. Lett. **82**, 445 (2003).

[12] Z. Zhong, A. Halilovic, T. Fromherz, F. Schaffler, and G. Bauer, Appl. Phys. Lett. **82**, 4779 (2003); Z. Zhong, W. Schwinger, F. Schäffler, G. Bauer, G. Vastola, F. Montalenti, and L. Miglio, Phys. Rev. Lett. **98**, 176102 (2007); M. Bollani, D. Chrastina, A. Fedorov, R. Sordan, A. Picco, and E. Bonera, Nanotechnology **21**, 475302 (2010); Y. J. Ma, Z. Zhong, X. J. Yang, Y. L. Fan, and Z. M. Jiang, *ibid.* **24**, 015304 (2013).

[13] I. Berbezier and A. Ronda, Surf. Sci. Rep. **64**, 47 (2009).

[14] R. V. Kukta and D. Kouris, J. Appl. Phys. **97**, 033527 (2005).

[15] A. Bavard, J. Eymery, A. Pascale, and F. Fournel, Phys. Status Solidi B **243**, 3963 (2006).

[16] G. Katsaros, J. Tersoff, M. Stoffel, A. Rastelli, P. Acosta-Diaz, G. S. Kar, G. Costantini, O. G. Schmidt, and K. Kern, Phys. Rev. Lett. **101**, 096103 (2008).

[17] T. U. Schülli, G. Vastola, M.-I. Richard, A. Malachias, G. Renaud, F. Uhlík, F. Montalenti, G. Chen, L. Miglio, F. Schäffler, and G. Bauer, Phys. Rev. Lett. **102**, 025502 (2009).

[18] G. Vastola, M. Grydlik, M. Brehm, T. Fromherz, G. Bauer, F. Boioli, L. Miglio, and F. Montalenti, Phys. Rev. B **84**, 155415 (2011).

[19] A. Pascale, I. Berbezier, A. Ronda, and P. C. Kelires, Phys. Rev. B **77**, 075311 (2008).

[20] H. Wang, Y. Zhang, and F. Liu, J. Appl. Phys. **104**, 054301 (2008).

[21] R. Bergamaschini, J. Tersoff, Y. Tu, J. J. Zhang, G. Bauer, and F. Montalenti, Phys. Rev. Lett. **109**, 156101 (2012).

[22] J.-N. Aqua and T. Frisch, Phys. Rev. B **82**, 085322 (2010).

[23] J.-N. Aqua, A. Gouyé, T. Auphan, T. Frisch, A. Ronda, and I. Berbezier, Appl. Phys. Lett. **98**, 161909 (2011).

[24] See, e.g., P. Müller and R. Kern, Appl. Surf. Sci. **102**, 6 (1996); C.-H. Chiu and H. Gao, in *Thin Films: Stresses and Mechanical Properties V*, edited by S. P. Baker *et al.*, MRS Symposia Proceedings No. 356 (Materials Research Society, Pittsburgh, 1995), p. 33.

[25] G.-H. Lu and F. Liu, Phys. Rev. Lett. **94**, 176103 (2005); O. E. Shklyaev, M. J. Beck, M. Asta, M. J. Miksis, and P. W. Voorhees, *ibid.* **94**, 176102 (2005).

[26] J.-N. Aqua, A. Gouyé, A. Ronda, T. Frisch, and I. Berbezier, Phys. Rev. Lett. **110**, 096101 (2013).

[27] J. Tersoff, B. J. Spencer, A. Rastelli, and H. von Känel, Phys. Rev. Lett. **89**, 196104 (2002).

[28] J.-N. Aqua, T. Frisch, and A. Verga, Phys. Rev. B **76**, 165319 (2007).

[29] J.-N. Aqua, T. Frisch, and A. Verga, Phys. Rev. E **81**, 021605 (2010).

[30] X. Xu, J.-N. Aqua, and T. Frisch, J. Phys.: Condens. Matter **24**, 045002 (2012); C. R. Phys. **14**, 199 (2013).

[31] C.-H. Lam, C.-K. Lee, and L. M. Sander, Phys. Rev. Lett. **89**, 216102 (2002).

[32] H. Hu, H. J. Gao, and F. Liu, Phys. Rev. Lett. **101**, 216102 (2008).

[33] P. Liu, C. Lu, and Y. W. Zhang, Phys. Rev. B **76**, 085336 (2007).

[34] J.-N. Aqua and T. Frisch, Phys. Rev. B **78**, 121305(R) (2008).

[35] P. Gaillard, J.-N. Aqua, and T. Frisch, Phys. Rev. B **87**, 125310 (2013).